Acta Crystallographica Section D
Biological Crystallography
ISSN 0907-4449

High-pressure cooling of protein crystals without cryoprotectants

Chae Un Kim,[a,b] Raphael Kapfer[c] and Sol M. Gruner[a,b,c]*

[a]Cornell High Energy Synchrotron Source (CHESS), USA, [b]Field of Biophysics, Cornell University, Ithaca, NY 14853-2501, USA, and [c]Physics Department, Cornell University, Ithaca, NY 14853-2501, USA

Correspondence e-mail: smg26@cornell.edu

Received 20 December 2004
Accepted 16 March 2005

Dedicated to Raphael Kapfer, who tragically passed away in a bicycle accident early on in the work.

Flash-cooling of protein crystals is the best known method to effectively mitigate radiation damage in macromolecular crystallography. To prevent physical damage to crystals upon cooling, suitable cryoprotectants must usually be found, a process that is time-consuming and in some cases unsuccessful. A method is described to cool protein crystals in high-pressure helium gas without the need for penetrative cryoprotectants. The method involves mounting protein crystals from the native mother liquor in a cryoloop with a droplet of oil, pressurizing the crystal to 200 MPa in He gas, cooling the crystal under pressure and then releasing the pressure. The crystal is then removed from the apparatus under liquid nitrogen and handled thereafter like a normal cryocooled crystal. Results are presented from three representative proteins. Dramatic improvement in diffraction quality in terms of resolution and mosaicity was observed in all cases. A mechanism for the pressure cooling is proposed involving high-density amorphous (HDA) ice which is produced at high pressure and is metastable at room pressure and 110 K.

1. Introduction

A typical protein crystal at room temperature only survives a fraction of the X-ray dose required for a complete high-resolution data set before it becomes irrevocably radiation-damaged. The mechanism of radiation damage is complex and includes both direct damage to protein molecules and secondary chemical degradation by the highly reactive free radicals created when water or other chemical additives are exposed to X-rays (Garman & Schneider, 1997). When a protein crystal is properly cryocooled, the molecular motions of both the polypeptide chains and the solvent in the crystal are damped to well below the glass transition and the diffusion of harmful free radicals is drastically reduced, allowing a typical 50–300 μm crystal to survive long enough in the X-ray beam to collect a complete high-resolution data set using a single crystal (Hope, 1988, 1990; Young *et al.*, 1993; Rodgers, 1994; Watowich *et al.*, 1995; Chayen *et al.*, 1996; Garman & Schneider, 1997; Garman, 1999).

The primary goal of cryocooling is to turn the water surrounding and inside the crystal into amorphous ice. Amorphous ice is necessary because crystalline ice yields spurious diffraction that obscures useful protein diffraction. The formation of amorphous ice, which requires exceedingly rapid temperature drops, is usually limited by the time it takes heat to diffuse out of a typical 50–300 μm diameter crystal (Kriminski *et al.*, 2003). To facilitate amorphous ice formation, chemical cryoprotectants such as glycerol or polyethylene glycol are usually added to the mother liquor (Garman &

Schneider, 1997). Another problem with cryocooling is that even with fully amorphous ice, the differential volume change of the mother liquor, protein and unit cell upon cooling degrades or totally destroys the diffraction quality of the crystal (Kriminski *et al.*, 2002; Juers & Matthews, 2004). A second benefit of a properly chosen cryoprotectant is that it limits this volume-related damage. In practice, cryoprotectants that work with one protein do not work with another, requiring a trial-and-error search for suitable cryoprotectant conditions. Unfortunately, there are few rules to guide this search; indeed, some crystals, such as crystals of viruses and large complexes, have never been successfully cryocooled. Even in cases where a suitable cryoprotectant is found, cooling usually degrades the crystal quality and increases the mosaic spread, thereby limiting the quality of the data set (Juers & Matthews, 2004). Moreover, the chemical reactions between cyroprotectants and molecules within the crystal cannot always be ruled out. Hence, care has to be taken in choosing a proper cryoprotectant agent for a specific protein crystal to minimize unwanted side effects such as cryoprotectant binding to the protein active site (Garman & Schneider, 1997).

An alternative cooling method was suggested by Thomanek *et al.* (1973). They pressurized myoglobin crystals to 250 MPa in isopentane prior to cooling, reasoning that such pressures would freeze water to ice III which contracts, in contrast to ice I which expands, thus protecting the crystal from damage. Although decent diffraction patterns were obtained from crystals removed from the isopentane using this procedure, to the best of our knowledge there was no further development of the technique. Almost 30 years later, Urayama *et al.* (2002) used a slightly modified version of this technique to study pressure-induced changes in the myoglobin structure. It was shown that the magnitude of the structural changes induced by pressure-cooling followed by cryocrystallography was comparable to the changes arising from flash-cooling at ambient pressure. The tedium of removing the pressure-cooled crystal from isopentane at liquid-nitrogen temperature led us to develop a more convenient method of pressure-cooling in helium gas. We now report on tests of this system using several protein crystals. In almost all cases, we observed a significant improvement in diffraction quality in terms of both mosaicity and resolution without any permeable cryoprotectants. A mechanism is proposed to explain why the method works.

2. Experimental

2.1. Cooling methods: flash-cooling at room pressure *versus* high-pressure cooling

2.1.1. Flash-cooling at room pressure. Crystals were transferred to NVH oil (catalog No. HR3-617, Hampton Research, Laguna Niguel, CA, USA) and swished back and forth to remove excess mother liquor on the surface of the crystals. The crystals were picked up in commercially available cryoloops (Hampton Research) with a minimal droplet of the oil. They were then flash-cooled by plunging directly into liquid nitrogen (LN_2; 77 K) at room pressure without using any penetrative cryoprotectants. The absence of cryoprotectants allows a direct comparison with the high-pressure cooling method, which also does not use cryoprotectants.

2.1.2. High-pressure cooling. The high-pressure cooling process is shown schematically in Fig. 1. Crystals were picked up in oil in cryoloops in the exactly same manner as in preparation for room-pressure flash-cooling. In the high-pressure cooling, the oil coating is essential to prevent dehydration of the crystals during the 25 min pressurizing process. The pressure-cooling apparatus is shown in Fig. 2. In brief, the cryoloop stud was inserted into one end of a small length of brass tubing partially filled with a short length of steel piano wire (Fig. 2*a*). This was then inserted into one end of a 30 cm straight length of heavy-wall stainless-steel high-pressure tubing (catalog No. 60-HM4-12, High Pressure Equipment Company, Erie, PA, USA) capped at the other end with an endcap. A strong magnet (rare-earth magnet, Hartville Tool, Hartville, OH, USA) placed on the outside of the high-pressure tubing attracted the piano wire inside and held the cryoloop assembly in place. The high-pressure tubing was placed into a special jig in a vertical position with the crystal at the top and the capped end at the bottom of an LN_2 container (Fig. 2*b*). The upper end of the tubing was then connected to a high-pressure He-gas compressor (catalog No. 46-13427-2, Newport Scientific, Jessup, MD, USA) using standard commercial high-pressure cone-seal fittings (High Pressure Equipment Company). A pressure of up to 200 MPa was applied to the crystals. Because stainless-steel tubing is a poor heat conductor, the upper end (crystals) remains above 283 K. The crystals were left under pressure for 25 min to equilibrate and then (while still under high pressure) dropped into the lower part of the tubing under LN_2 by removing the magnet holding the cryoloop assembly. After 10 min, pressure was released and the high-pressure connections to the pump were unscrewed, leaving the crystals with the bottom endcaps in the LN_2 container. Simple homemade fixtures were used to

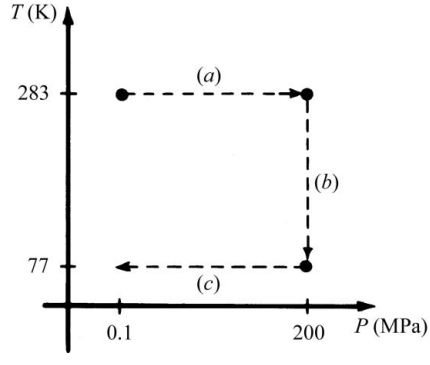

Figure 1
Simplified diagram of the high-pressure cooling method. (*a*) Pressurization to 200 MPa at 283 K using He-gas compressor. Crystals are left under pressure for 25 min to equilibrate. (*b*) Cooling crystals under pressure by dropping samples to the lower part of pressure tubing immersed in LN_2 (77 K). (*c*) After 10 min, pressure is released while the samples are kept cooled at 77 K. Crystals are stored in a LN_2 dewar until data collection at low temperature and ambient pressure.

disassemble the remaining tubing in the LN_2 container. The cooled crystals in their cryoloops were then transferred into crystalcaps (Hampton Research) under LN_2 and stored in an LN_2 dewar until data collection at room pressure.

The pressure-cooling apparatus described above consists primarily of a commercially available high-pressure gas compressor and off-the-shelf high-pressure plumbing and gauges. The assembly and disassembly required to freeze crystals is performed with simple hand wrenches and home-made jigs. We typically can pressure-freeze several crystals an hour. To date, hundreds of crystals of about a dozen proteins have been successfully cooled. Obviously, with some effort the apparatus can be engineered with quick-disconnect high-pressure fittings for more effective throughput.

It is important to note that helium gas expands by almost 2000 times when released into air from 200 MPa. This tremendous explosive power necessitates great caution. For safety reasons, our apparatus is enclosed in a half-inch-thick carbon-steel container. This, in turn, is housed in a cinder-block utility room (Fig. 2*c*). All high-pressure operations are performed without personnel present in the room, *via* remotely controlled monitors, switches, motors and pulleys.

2.2. Materials and data collection

Three kinds of protein crystals were prepared by both flash-cooling at room pressure and high-pressure cooling. Diffraction data were collected at the Cornell High Energy Synchrotron Source (CHESS) on beamline F1 (λ = 0.9186 Å, ADSC Quantum-4 CCD detector) and F2 (λ = 0.9795 Å, ADSC Quantum-210 CCD detector). In all cases the detector face was perpendicular to the incident beam (2θ value of zero). All data were collected at 110 K (N_2-gas stream) and room pressure with oscillation angle ($\Delta\varphi$) 1.0°.

2.2.1. Glucose isomerase. Glucose isomerase from *Streptomyces rubiginosus* (catalog No. HR7-102) was purchased from Hampton Research and dialyzed against pure water before crystallization. Crystals were grown by the hanging-drop method by mixing 2 µl of a reservoir solution containing 1.15 *M* ammonium sulfate, 1 m*M* magnesium sulfate and 10 m*M* HEPES pH 7.5 with 2 µl 25 mg ml^{-1} protein solution in pure water (modified from Carrell *et al.*, 1989). The crystals appeared in a few days and grew to maximum size (1 × 1 × 1 mm) in a week. Approximately 250 µm sized crystals were used for data collection. Data were collected at CHESS F2 station (beam diameter = 150 µm). The first image (Fig. 3*a*) corresponds to the crystal flash-cooled at room pressure. The distance between the crystal and detector (*d*) was 150 mm and the exposure time was 60 s. Four consecutive images were collected to estimate resolution and mosaicity. The second image (Fig. 3*b*) corresponds to the crystal pressure-cooled at 130 MPa. The distance was 150 mm and the exposure time was 30 s. A data set containing 155 frames was collected for structure determination.

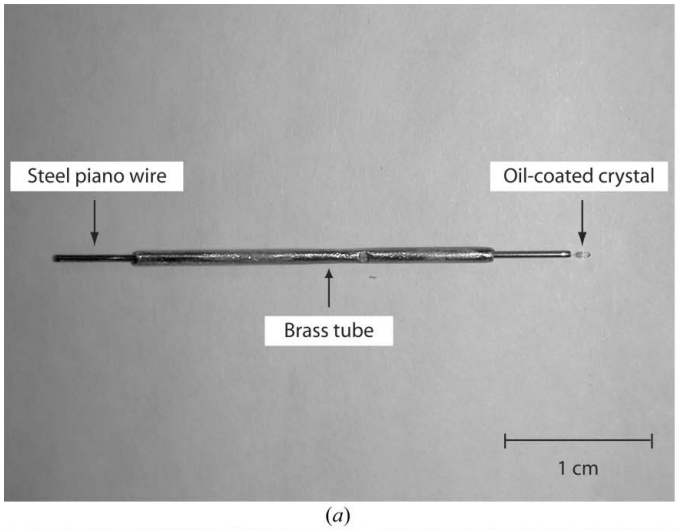

(*a*)

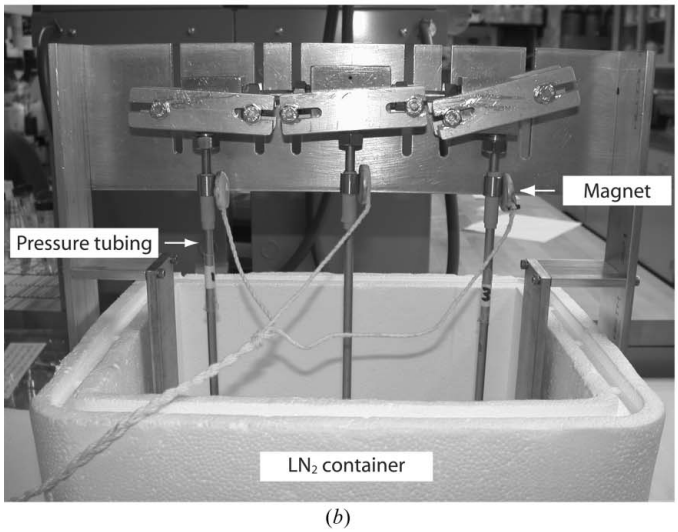

(*b*)

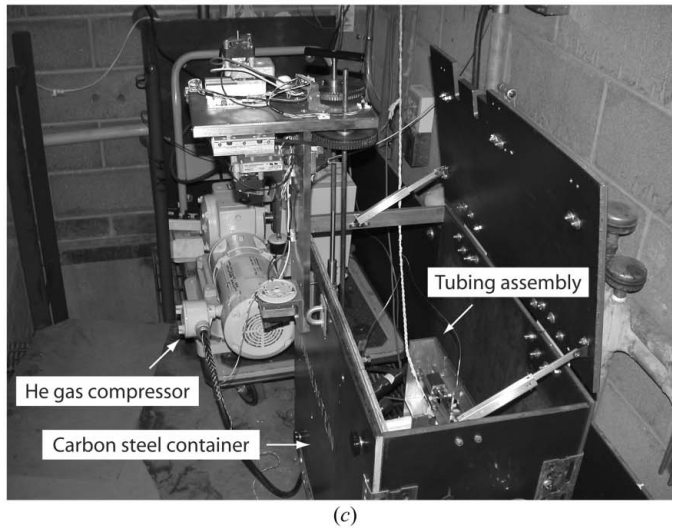

(*c*)

Figure 2
High-pressure cooling apparatus. (*a*) Sample pin. An oil-coated crystal in a cryoloop is inserted into one end (right) of a brass tube (2.5 cm long) and a steel piano wire in the other end (left). (*b*) High-pressure tubing assembly in a LN_2 container. A sample is loaded into the top of each 30 cm long tube and is held in place by a magnet outside the tube. Three crystals can be pressure-cooled at a time. (*c*) High-pressure tubing assembly in a carbon-steel container. The assembly is connected to a He-gas compressor (rear). All high-pressure operations are controlled remotely for safety reasons.

2.2.2. Thaumatin. Thaumatin from *Thaumatococcus daniellii* (catalog No. T7638) was purchased from Sigma (Saint Louis, MO, USA) and used for crystallization without further purification. Crystals were grown by the hanging-drop method by mixing 2 µl of a reservoir solution containing 0.9 *M* sodium potassium tartrate with 2 µl 25 mg ml^{-1} protein solution in

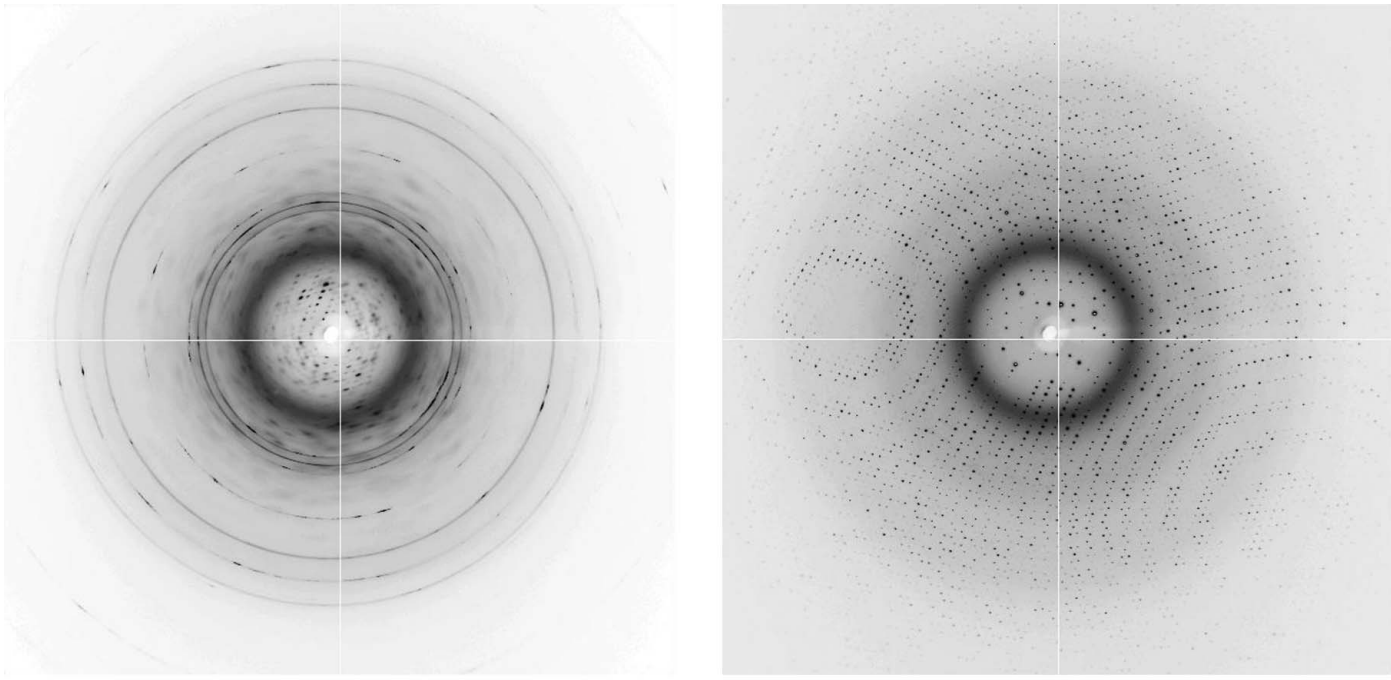

(*a*) (*b*)

Figure 3
Glucose isomerase. (*a*) Diffraction image of a crystal flash-cooled at ambient pressure (λ = 0.9795 Å, beam diameter = 150 µm, Δφ = 1.0°, *d* = 150 mm, 60 s). Strong ice rings are seen. The diffraction resolution is 5.0 Å and the mosaicity is very poor. (*b*) Diffraction image of a crystal pressure-cooled at 130 MPa (λ = 0.9795 Å, beam diameter = 150 µm, Δφ = 1.0°, *d* = 150 mm, 30 s). The diffraction resolution reaches 1.3 Å and the mosaicity is 0.39°.

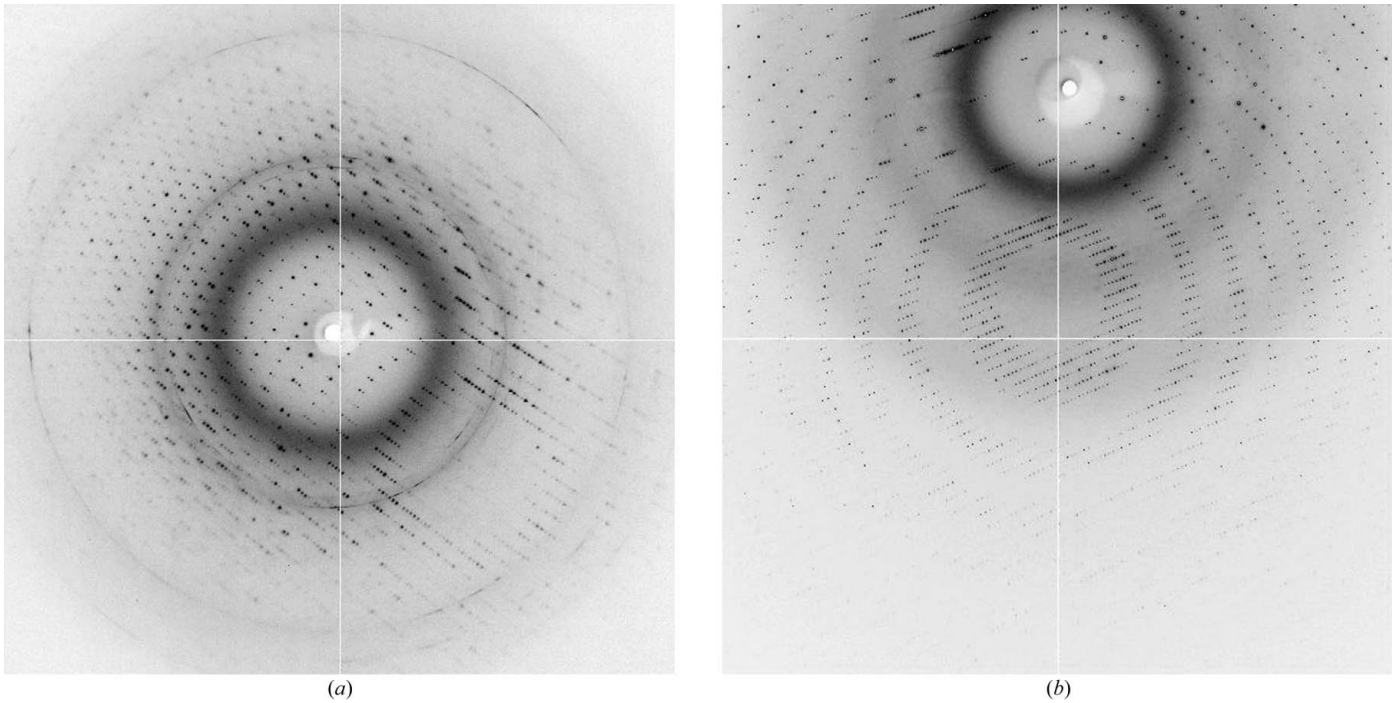

(*a*) (*b*)

Figure 4
Thaumatin. (*a*) Diffraction image of a crystal flash-cooled at ambient pressure (λ = 0.9795 Å, beam diameter = 100 µm, Δφ = 1.0°, *d* = 200 mm, 20 s). Ice rings are seen. The diffraction resolution is 1.8 Å and the mosaicity is 1.29°. (*b*) Diffraction image of a crystal pressure-cooled at 185 MPa (λ = 0.9186 Å, beam diameter = 100 µm, Δφ = 1.0°, *d* = 175 mm, 15 s). The diffraction resolution reaches 1.15 Å and the mosaicity is 0.11°.

50 m*M* HEPES buffer pH 7.0 (modified from Ko *et al.*, 1994). The crystals appeared in a day and grew to maximum size (150 × 250 × 500 µm, truncated bipyramidal shape) in a week. The first image (Fig. 4*a*) corresponds to the crystal flash-cooled at room pressure and was collected at CHESS F2 station (beam size = 100 µm, *d* = 200 mm and exposure time = 20 s). Four consecutive images were collected to estimate the resolution and mosaicity. The second image (Fig. 4*b*) corresponds to the crystal pressure-cooled at 185 MPa and was collected at CHESS F1 station (beam size = 100 µm, *d* = 175 mm and exposure time = 15 s). A data set containing 200 frames was collected.

2.2.3. AHP-LAAO. AHP-LAAO (L-amino-acid oxidase from *Agkistrodon halys pallas*) protein solution was kindly provided by H. Zhang and L. Niu. Crystals were grown by the hanging-drop method by mixing 1 µl of a reservoir solution containing 2 *M* ammonium sulfate and 0.1 *M* sodium citrate pH 5.0 with 2 µl 40 mg ml^{-1} protein solution in pure water (modified from Zhang *et al.*, 2004). The crystals appeared in two weeks and grew to maximum size (50 × 100 × 100 µm) after one month. Data were collected at CHESS F2 station (beam diameter = 150 µm). The first image (Fig. 5*a*) corresponds to the crystal flash-cooled at room pressure. The distance was 200 mm and the exposure time was 60 s. Four consecutive images were collected to estimate resolution and mosaicity. The second image (Fig. 5*b*) corresponds to the crystal pressure-cooled at 190 MPa. The distance was 250 mm and the exposure time was 60 s. A data set containing 60 frames was collected.

2.3. Data processing and structure determination

The data were processed with *DPS*/*MOSFLM* (Steller *et al.*, 1997; Leslie, 1992) and scaled with *SCALA* (Collaborative Computational Project, Number 4, 1994). The mosaicity of each data set was determined in the *MOSFLM* refinement process using four consecutive images. The initial structures were determined by the molecular-replacement method using the program *MOLREP* (Vagin & Teplyakov, 1997) from the *CCP*4 program suite (Collaborative Computational Project, Number 4, 1994). The structures were then refined using the data sets with *REFMAC*5 (Murshudov *et al.*, 1997; Collaborative Computational Project, Number 4, 1994). Water molecules were automatically located and ($F_o - F_c$) and ($2F_o - F_c$) maps were generated during the refinement process. The difference maps were displayed with the *Xtalview*/*Xfit* program (McRee, 1999) for model corrections. Structural figures were produced using *PyMol* (DeLano, 2002).

3. Results

3.1. Glucose isomerase

The crystal flash-cooled at room pressure diffracted to only 5.0 Å and spots were severely smeared (Fig. 3*a*). The image was not auto-indexable and mosaicity could not be estimated. The crystal looked entirely white and cloudy in the cold stream and very intense ice rings were seen in the image, indicating that much water had turned into crystalline ice

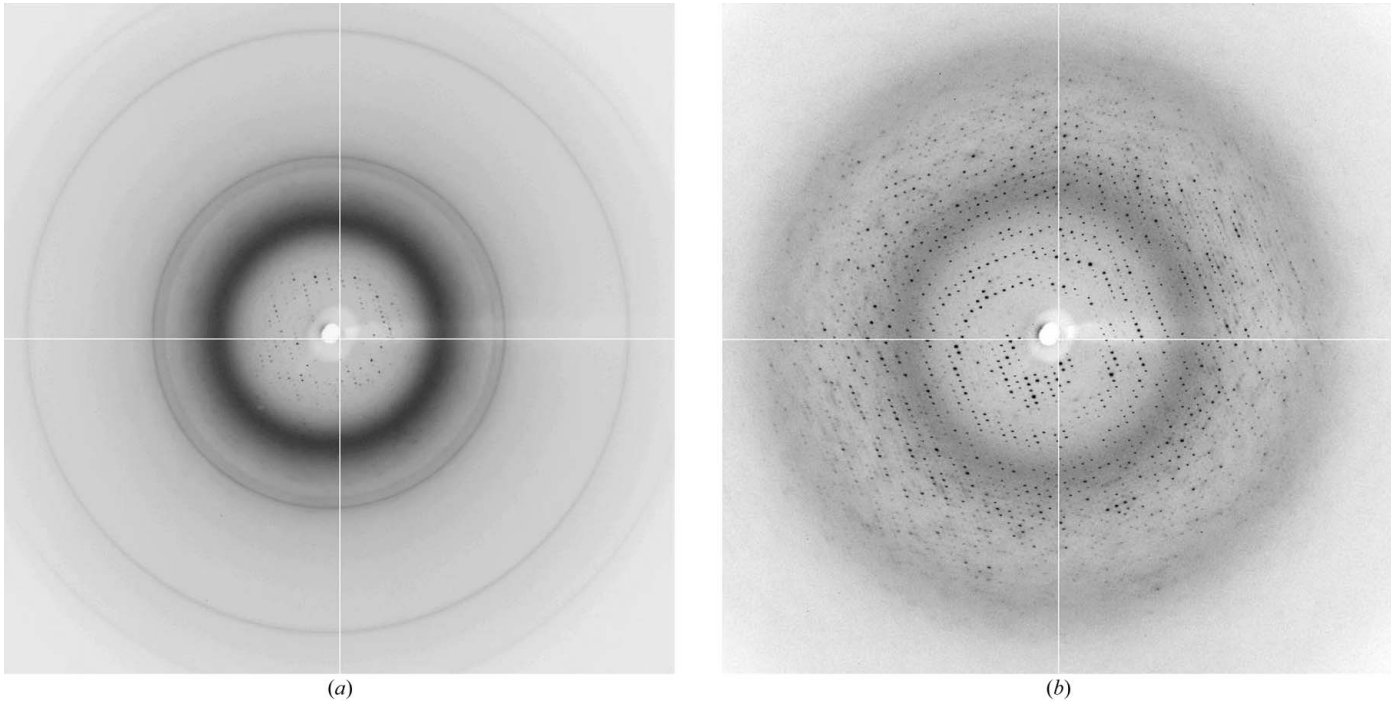

(*a*) (*b*)

Figure 5
AHP-LAAO. (*a*) Diffraction image of a crystal flash-cooled at ambient pressure (λ = 0.9795 Å, beam diameter = 150 µm, Δφ = 1.0°, *d* = 200 mm, 60 s). Strong ice rings are seen. The diffraction resolution is only 7.0 Å and the mosaicity is very poor. (*b*) Diffraction image of a crystal pressure-cooled at 190 MPa (λ = 0.9795 Å, beam diameter = 150 µm, Δφ = 1.0°, *d* = 250 mm, 60 s). The diffraction resolution reaches 2.7 Å and the mosaicity is 0.56°.

Table 1
Summary of crystallographic statistics.

Values in parentheses are for the last shell.

	Glucose isomerase (130 MPa)	Thaumatin (185 MPa)	AHP-LAAO (190 MPa)
Space group	$I222$	$P4_12_12$	$I2_13$
Unit-cell parameters (Å)	a = 92.9, b = 98.7, c = 102.6	$a = b$ = 58.0, c = 151.1	$a = b = c$ = 167.9
Solvent content (%)	54.7	56.7	61.8
Resolution range (Å)	30–1.45 (1.53–1.45)	30–1.5 (1.58–1.5)	30–2.9 (3.06–2.9)
No. of observations	437820 (28611)	300340 (35155)	127586 (17208)
No. of unique reflections	82638 (11314)	41519 (5569)	17583 (2535)
Multiplicity	5.3 (2.5)	7.2 (6.3)	7.3 (6.8)
Completeness (%)	99.1 (94.3)	98.1 (92.3)	99.9 (99.9)
R_{sym} (%)	7.2 (20.9)	10.5 (26.0)	12.3 (38.2)
$I/\sigma(I)$	16.5 (4.0)	13.3 (6.6)	14.0 (3.7)
R factor (%)	17.6	17.5	
R_{free} factor (%)	19.8	20.2	
Average B factor (Å^2)	13.0	13.7	
No. of water molecules	773	486	
R.m.s. deviation from ideality			
Bond lengths (Å)	0.011	0.013	
Angles (°)	1.331	1.389	

during the flash-cooling process at atmospheric pressure (0.1 MPa). The diffraction images from several crystals prepared by the flash-cooling method at 0.1 MPa were no better than this image. On the other hand, the crystal pressure-cooled at 130 MPa diffracted to 1.3 Å with 0.39° mosaicity (Fig. 3*b*). An overexposed snapshot image (90 s) was collected at a closer distance (100 mm) to check the diffraction limit and the diffraction spots reached the maximum resolution area (1.05 Å) of the image (figure not shown). The pressure-cooled crystal looked clear and transparent and no ice rings were observed, indicating that crystalline ice formation was entirely suppressed by pressure without any penetrative cryoprotectants. The average resolution and mosaicity of three different crystals prepared by high-pressure cooling at 130 MPa were 1.3 Å (at least) and 0.48°, respectively.

The pressure-cooled crystal belonged to the body-centered orthorhombic space group $I222$, with unit-cell parameters a = 92.9, b = 98.7, c = 102.6 Å. There was one monomer in an asymmetric unit and the solvent content was 54.7% (Matthews coefficient V_M = 2.7 Å^3 Da^{-1}; Matthews, 1968). The structure (PDB code 8xia) from Carrell *et al.* (1989) was employed as a starting model for molecular replacement. In the final model, the crystallographic R factor and R_{free} factor converged to 17.6 and 19.8%, respectively, at 1.45 Å. Details of the data-collection statistics and structure-refinement statistics are listed in Table 1.

3.2. Thaumatin

The crystal flash-cooled at room pressure diffracted to 1.8 Å with 1.29° mosaicity (Fig. 4*a*). Ice rings are seen in the diffraction image and the crystal looked slightly cloudy, indicating that water was not entirely vitrified during the flash-cooling process at 0.1 MPa. The average resolution and mosaicity of three different flash-cooled crystals were 1.93 Å and 1.4°, respectively. On the other hand, the crystal pressure-cooled at 185 MPa diffracted to 1.15 Å with 0.11° mosaicity (Fig. 4*b*). Crystalline ice formation was completely suppressed by pressure, as no ice rings appeared in the image. The pressure-cooled crystals looked transparent, unlike the flash-cooled ones. The average resolution and mosaicity of four different crystals prepared by high-pressure cooling at 185–190 MPa were 1.35 Å and 0.3°, respectively.

The crystal flash-cooled at room pressure (Fig. 4*a*) belonged to the primitive tetragonal space group $P4_12_12$, with unit-cell parameters $a = b$ = 58.3, c = 149.8 Å. The pressure-cooled crystal (Fig. 4*b*) belonged to the same space group, with unit-cell parameters $a = b$ = 58.0, c = 151.1 Å. There was one molecule in an asymmetric unit and the solvent content was 56.7% (Matthews coefficient V_M = 2.9 Å^3 Da^{-1}; Matthews, 1968) for the pressure-cooled crystal. The structure (PDB code 1lxz) from Charron *et al.* (2002) was employed as a starting model for molecular replacement. In the final model, the crystallographic R factor and R_{free} factor converged to 17.5 and 20.2%, respectively, at 1.5 Å. Details of the data-collection statistics and structure-refinement statistics are listed in Table 1.

3.3. AHP-LAAO

The crystal flash-cooled at room pressure diffracted to only 7.0 Å and strong ice rings were produced (Fig. 5*a*). The image was not auto-indexable and mosaicity could not be estimated. Another crystal prepared by flash-cooling gave a diffraction image even poorer than this one. On the other hand, the crystal pressure-cooled at 190 MPa diffracted to 2.7 Å with 0.56° mosaicity (Fig. 5*b*). No ice rings were observed and crystalline ice formation was suppressed by pressure, as for the glucose isomerase crystals. The average resolution and mosaicity of three different crystals prepared by high-pressure cooling at 190 MPa were 2.7 Å and 0.59°, respectively.

The pressure-cooled crystal belonged to the body-centered cubic space group $I2_13$, with unit-cell parameters $a = b = c$ = 167.9 Å. There was one molecule in an asymmetric unit and the solvent content was 61.8% (Matthews coefficient V_M = 3.2 Å^3 Da^{-1}; Matthews, 1968). Details of the data-collection statistics are listed in Table 1.

4. Discussion

The suppression of crystalline ice at ambient pressure typically requires either extremely rapid cooling or the addition of cryoprotectants. Pressure cooling appears to suppress the formation of crystalline ice. Indeed, Urayama *et al.* (2002)

found that myoglobin crystals were successfully cryocooled without ice formation at high pressure (150 MPa) even when cooled at only a degree or two per second. The reason that the cooling rate appears to be more forgiving at high pressures is not fully understood, but we make the following hypothesis. As shown in the temperature–pressure phase diagram of water (Fig. 6), the melting point and the water supercooled region decrease as pressure increases up to 210 MPa. Furthermore, the nucleation and growth of ice I (hexagonal or cubic ice) is suppressed because the higher density of liquid water is favored at high pressure (Le Chatelier's principle). Another type of crystalline ice, ice II, is allowed at high pressure. However, the nucleation and growth rates of ice II at high pressure are initially slower than those of ice I at ambient pressure, even though ice II has a smaller volume than liquid water (Franks, 1982).

Crystal degradation during normal flash-cooling occurs for several reasons. When crystals are cooled, the unit-cell volume usually shrinks by 2–7% as a result of molecular rearrangement in the protein packing (Juers & Matthews, 2001).

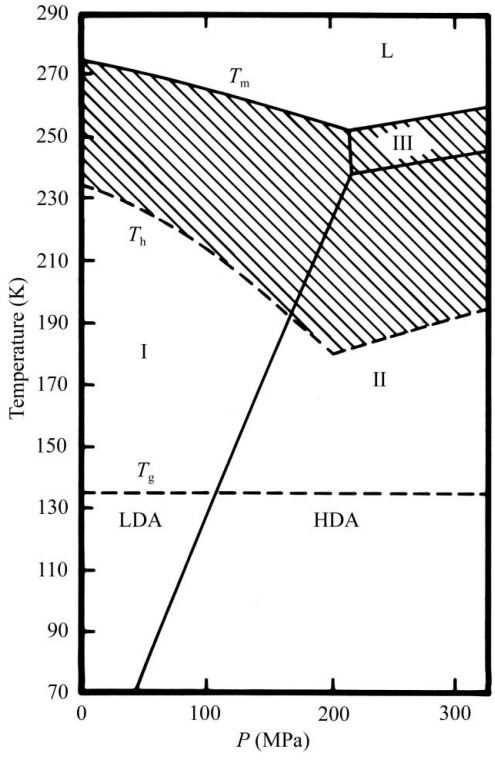

Figure 6
The pressure–temperature phase diagram of H_2O [adapted from Kanno *et al.* (1975), Franks (1985), Garman & Schneider (1997) and Mishima & Stanley (1998)]. Amorphous ices form when liquid water is rapidly cooled below the glass-transition temperature (T_g), preventing the nucleation and growth of crystalline ices. HDA ice may form upon cooling above ~100 MPa. LDA ice is formed below ~100 MPa. The hatched region is the allowed region for supercooled liquid water. The melting point (T_m) and the lowest temperature (T_h) for supercooled water both decrease with pressure up to 210 MPa. The region in which the amorphous phase can exist depends on the thermal/pressure history of the system. HDA ice is metastable at ambient pressure as long as the temperature is kept below 120 K. Note that the glass-transition line (T_g) is very hard to determine exactly experimentally and should be taken as an estimate.

The protein molecule itself contracts as well (1–2%), but much less than the unit cell. These effects reduce the volume available for water in the crystal. However, normal crystalline ice (ice I) has a larger volume per water molecule (*i.e.* a lower density) than liquid water. When low-density amorphous (LDA) ice forms at ambient pressure, although it produces no ice-diffraction rings, the amorphous ice also expands relative to liquid water. In fact, the 6.7% volume expansion of LDA ice (0.94 g cm^{-3} at 77 K, 0.1 MPa) is almost the same as that of hexagonal ice I at liquid-nitrogen temperature (Ghormley & Hochanadel, 1971; Röttger *et al.*, 1994). These conflicting tendencies (shrinking of the available water volume and the water expansion) lead to crystal disruption. Therefore, at room pressure suitable cryoprotectants must be found not only to suppress crystalline ice formation but also to raise the density of the resultant amorphous water.

We propose that the improvement in diffraction quality during high-pressure cooling involves the formation of high-density amorphous (HDA) ice. When cooled at high pressures, liquid water may freeze directly into HDA ice and, once formed, stays metastably in the HDA state when the pressure is removed, as long as the temperature is kept below 120 K (Mishima *et al.*, 1984). In contrast to ice I and LDA ice, HDA ice has a significantly higher density (1.17 g cm^{-3} at 77 K, 0.1 MPa). As a result, HDA ice at 0.1 MPa occupies less volume per molecule than liquid water at 0.1 MPa. This helps mitigate crystal disruption. Glucose isomerase crystals pressure-cooled at several different pressures support this explanation. A clue that HDA ice is involved is the observation that crystals pressure-cooled below ~100 MPa, where the LDA ice can form (see Fig. 6), consistently diffracted to worse than 3.0 Å resolution (Fig. 7*a*), whereas crystals pressure-cooled above ~100 MPa consistently diffracted to better than 1.3 Å (Fig. 7*b*). Verification of the HDA hypothesis, for example, by neutron-scattering studies of the vitrified water, is beyond the scope of this paper.

This paper reports detailed results of pressure-cooling three different types of protein crystals. The method has also been systematically applied to ten other proteins (data not shown). In all cases except one, water vitrification and acceptable crystal diffraction was achieved without penetrative cryoprotectants. The exceptional case was deoxyhemoglobin, where the pressure-cooled crystals consistently diffracted poorly compared with the crystals flash-cooled at room pressure.

It is interesting to note that most protein crystals readily survive pressurization. It has been reported that tetragonal hen egg-white lysozyme crystals grown at low salt concentration (0.83 *M* NaCl) cracked when pressurized with mother liquor in a beryllium pressure cell at 30–40 MPa (Kundrot & Richards, 1987). However, in our apparatus, lysozyme crystals grown in 0.8 *M* NaCl did not crack under pressures up to 200 MPa. Our observations are that crystal cracking is rare during helium high-pressure cooling.

In practice, high-pressure cooling is an effective approach to the cryoprotection of protein crystals without the need for penetrative cryoprotectants. Zhang *et al.* (2004) tried to cryocool AHP-LAAO protein crystals by normal flash-cooling

methods with cryoprotectants, but the flash-cooled crystals diffracted to worse than 5 Å. As described earlier, the AHP-LAAO crystals pressure-cooled at 190 MPa diffracted to 2.7 Å without any penetrative cryoprotectants.

Structural perturbations in proteins arising from pressure are generally small, but must be kept in mind. Kundrot & Richards (1987) reported very small structural shifts in lysozyme at room temperature and 100 MPa. This small structural change in lysozyme was confirmed by an NMR solution study (Refaee *et al.*, 2003). Urayama *et al.* (2002) performed a careful analysis on myoglobin and also measured very small differences at the level of shifts of protein secondary-structure blocks by 0.1–0.4 Å when proteins are either flash-cooled at room pressure or pressure-cooled in liquid isopentane. In order to investigate the perturbation of protein structures by He-gas high-pressure cooling, the initial structures were determined by molecular replacement using the known atmospheric pressure protein coordinates in the PDB and then refined against the diffraction data sets as described in §2.3. The results are shown in Fig. 8 (AHP-LAAO is not presented in this paper simply because the structural difference might be biased by the relatively low-resolution structures). For glucose isomerase, the superposition of the flash-cooled structure (PDB code 8xia; 285–288 K, 0.1 MPa; Carrell *et al.*, 1989) and the pressure-cooled structure (110 K, 130 MPa) shows little difference (Fig. 8*a*). The r.m.s. deviation between the C^{α} backbone atoms in the two models is 0.327 Å and the r.m.s. deviation between all atoms is 0.459 Å. For thaumatin, the superposition of the flash-cooled structure (PDB code 1lxz ; 100 K, 0.1 MPa; Charron *et al.*, 2002) and the pressure-cooled structure (110 K, 185 MPa) also shows only very small changes (Fig. 8*b*). The r.m.s. deviation between C^{α} atoms in the two models is 0.299 Å and the r.m.s. deviation between all atoms is 0.472 Å. Overall, the evidence so far suggests that the magnitude of structural perturbation upon pressure cooling is typically comparable with the small perturbations that are always observed upon lowering temperature, *e.g.* upon flash-cooling independent of pressure. The inference, by extension, is that most proteins do not show large-scale structural perturbations under our pressure-cooling conditions.

It is known that pressure certainly perturbs many proteins in solution. There is a large amount of literature demonstrating that pressures encountered in the biosphere (<130 MPa) have large effects on the functioning of many proteins (Unno *et al.*, 1990; Moss *et al.*, 1991; Jung, 2002; Verkhusha *et al.*, 2003). At some level of resolution, these functional perturbations must be manifest as structural perturbations. As mentioned above, in most cases pressures below 200 MPa seem to only slightly perturb protein backbone structures, involving atomic displacements of a few tenths of an angstrom. The fact that a structural perturbation is small does not necessarily mean that the functional effect is also small. For example, recall that the spatial displacements of the heme group upon binding of oxygen in hemoglobin or myoglobin are under 1 Å.

Similarly, the structural perturbations caused by simply cooling to liquid-nitrogen temperature, which are generally of

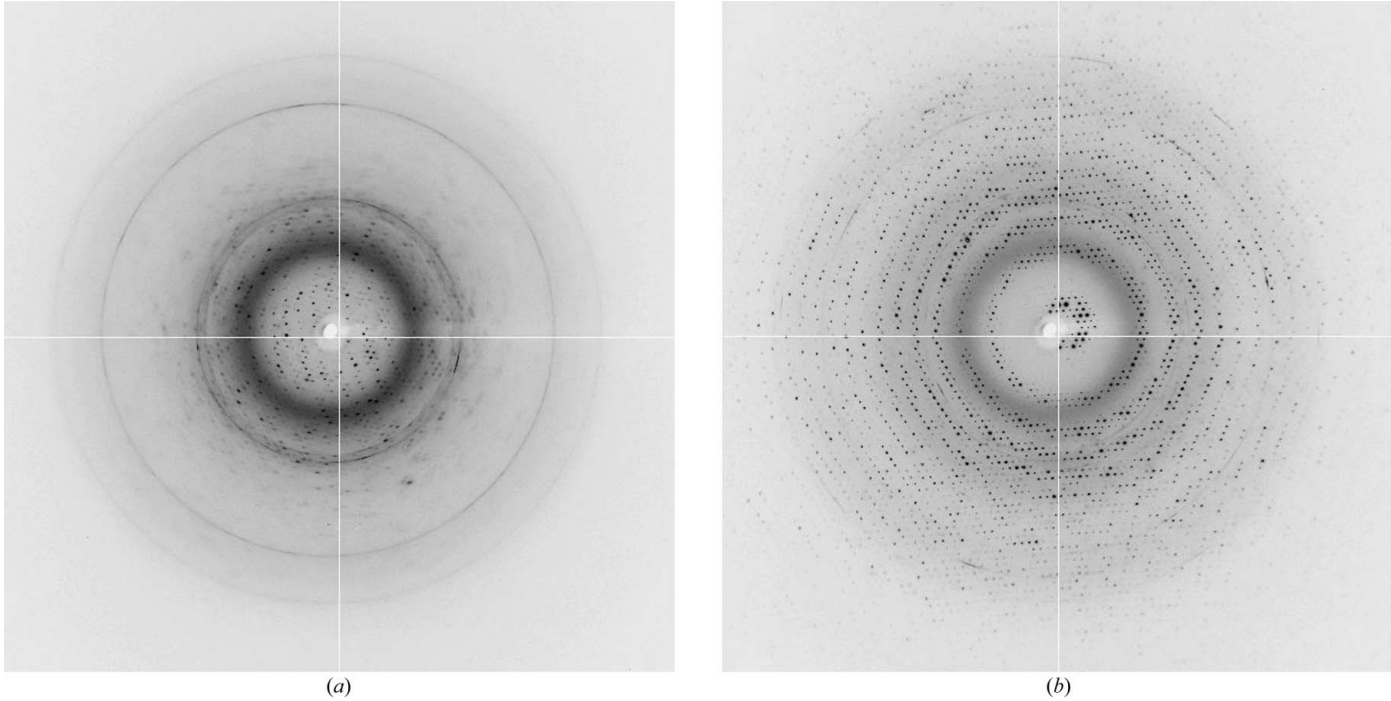

(*a*) (*b*)

Figure 7
Glucose isomerase at different pressures (λ = 0.9795 Å, beam diameter = 150 µm, $\Delta\varphi = 1.0^{\circ}$, d = 150 mm, 30 s). (*a*) Diffraction image of a crystal pressure-cooled at 90 MPa. The diffraction resolution is only 3.0 Å. (*b*) Diffraction image of a crystal pressure-cooled at 110 MPa. The diffraction resolution is 1.3 Å. Note that relatively faint ice rings are seen in both images, indicating that water vitrification is not entirely achieved at these modest pressure levels. See Fig. 3(*b*) for glucose isomerase pressure-cooled at 130 MPa.

similar magnitude, would likely have enormous consequences for protein function if only these effects were not masked by the cooling of water and the peptide glass transition. This comes as no surprise. The functions of many proteins are dramatically sensitive to temperature changes above 273 K. Yet the corresponding changes in structure may be small and may not be straightforward to understand in functional terms (Weber & Drickamer, 1983).

An analogy is useful here. Imagine that one wanted to understand an automobile gasoline engine but knew nothing about engines other than that they delivered rotary power to a car. Imagine that one had the static three-dimensional structures at 1 mm resolution of two almost identical engines. The only differences between the two engines are that one has a spark-plug gap expanded by a few tenths of a millimetre and the cylinders out of round by a few tenths of a millimetre. Since so little was known *a priori* about engines, either structure would be greatly and equally helpful in understanding how engines worked, because it would be possible to identify the parts of the engine, their relative positions and from this perhaps infer how mechanical power were generated. If one now tried to operate the two engines, it would become apparent that one operates very much worse than the other, if it operates at all. Would the two structural maps allow one to understand why one engine functions differently to the other? It can be achieved only with great difficulty, because the level of structural difference is below the observed resolution. Understanding at this level would involve either higher resolution or experimentation of what happens, for instance, when the gaps of the spark plugs are intentionally changed or inferences based on small changes in a relatively large mass (*e.g.* a piston out of round).

In summary, high-pressure cooling is a promising approach for crystals that are difficult to flash-cool by conventional methods; this method is now being used by CHESS users. The level of structural perturbation induced by pressure cooling is small in all cases examined so far, typically a few tenths of an angstrom. In terms of an overall structural determination, which is the object of the majority of crystallographic experiments, this level of perturbation is acceptable and is of the same magnitude as the perturbations induced by cooling to cryogenic temperatures. However, in terms of the detailed structure that might occur, for instance, around active sites, the effect of such small perturbations may not be negligible.

(*a*)

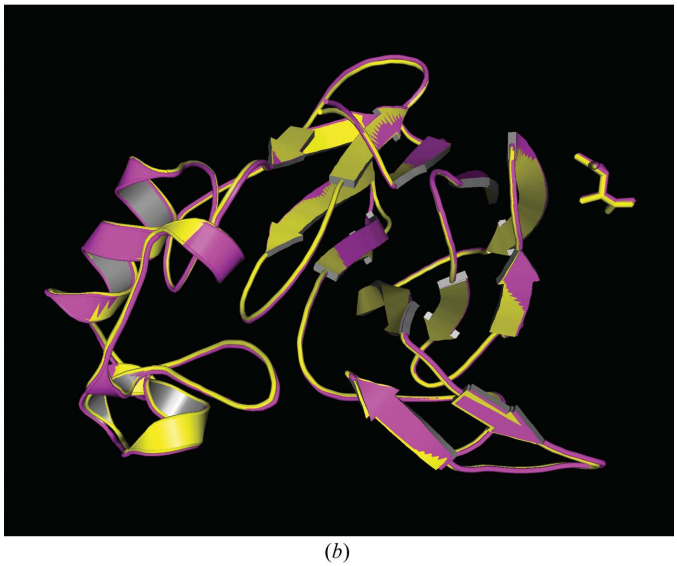

(*b*)

Figure 8
(*a*) Superposition of the room-pressure glucose isomerase structure (yellow) from 8xia (Carrell *et al.*, 1989) and the pressure-cooled structure (magenta). The r.m.s. deviation between C^{α} atoms in the two model is 0.327 Å and the r.m.s. deviation between all atoms is 0.459 Å. (*b*) Superposition of the room-pressure cooled thaumatin structure (yellow) from 1lxz (Charron *et al.*, 2002) and the pressure-cooled structure (magenta). The r.m.s. deviation between C^{α} atoms in the two model is 0.299 Å and the r.m.s. deviation between all atoms is 0.472 Å. These structural deviations are comparable to the structural change on dropping the temperature.

We thank Buz Barstow, Hye Won Chung and the MacCHESS staff for assistance in data collection, Gil Toombes and Quan Hao for comments, Hongmin Zhang and Liwen Niu for the AHP-LAAO protein solution, Jan Kmetko for information on protein crystallization and Seong A. Kang, Sang-Youn Park and Brian R. Crane for assistance in structure determination. This work was supported by the MacCHESS grant (US NIH grant RR 001646) and by US DOE grant DE-FG02-97ER62443 and CHESS, which is supported by the US NSF and NIH-NIGMS through NSF grant DMR-0225180.

References

Carrell, H. L., Glusker, J. P., Burger, V., Manfre, F., Tritsch, D. & Biellmann, J.-F. (1989). *Proc. Natl Acad. Sci. USA*, **86**, 4440–4444.
Charron, C., Kadri, A., Robert, M.-C., Giegé, R. & Lorber, B. (2002). *Acta Cryst.* D**58**, 2060–2065.
Chayen, N. E., Boggon, T. J., Cassetta, A., Deacon, A., Gleichmann, T., Habash, J., Harrop, S. J., Helliwell, J. R., Nieh, Y. P., Peterson, M. R., Raftery, J., Snell, E. H., Hadener, A., Niemann, A. C., Siddons, D. P., Stojanoff, V., Thompson, A. W., Ursby, T. & Wulff, M. (1996). *Q. Rev. Biophys.* **29**, 227–278.
Collaborative Computational Project, Number 4 (1994). *Acta Cryst.* D**50**, 760–763.
DeLano, W. (2002). *PyMol.* DeLano Scientific, San Carlos, CA, USA.

Franks, F. (1982). Editor. *Water – A Comprehensive Treatise*, Vol. 7, pp. 215–338. New York: Plenum.
Franks, F. (1985). *Biophysics and Biochemistry at Low Temperature.* Cambridge University Press.
Garman, E. (1999). *Acta Cryst.* D**55**, 1641–1653.
Garman, E. F. & Schneider, T. R. (1997). *J. Appl. Cryst.* **30**, 211–237.
Ghormley, J. A. & Hochanadel, C. J. (1971). *Science*, **171**, 62–64.
Hope, H. (1988). *Acta Cryst.* B**44**, 22–26.
Hope, H. (1990). *Annu. Rev. Biophys. Biophys. Chem.* **19**, 107–126.
Juers, D. H. & Matthews, B. W. (2001). *J. Mol. Biol.* **311**, 851–862.
Juers, D. H. & Matthews, B. W. (2004). *Q. Rev. Biophys.* **37**, 1–15.
Jung, C. (2002). *Biochem. Biophys. Acta*, **1595**, 309–328.
Kanno, H., Speedy, R. J. & Angell, C. A. (1975). *Science*, **189**, 880–881.
Ko, T.-P., Day, J., Greenwood, A. & McPherson, A. (1994). *Acta Cryst.* D**50**, 813–825.
Kriminski, S., Caylor, C. L., Nonato, M. C., Finkelstein, K. D. & Thorne, R. E. (2002). *Acta Cryst.* D**58**, 459–471.
Kriminski, S., Kazmierczak, M. & Thorne, R. E. (2003). *Acta Cryst.* D**59**, 697–708.
Kundrot, C. E. & Richards, F. M. (1987). *J. Mol. Biol.* **193**, 157–170.
Leslie, A. G. W. (1992). *Jnt CCP4–ESRF/EACBM Newsl. Protein Crystallogr.* **26**.
McRee, D. (1999). *J. Struct. Biol.* **125**, 156–165.
Matthews, B. W. (1968). *J. Mol. Biol.* **33**, 491–497.
Mishima, O., Calvert, L. D. & Whalley, E. (1984). *Nature (London)*, **310**, 393–395.
Mishima, O. & Stanley, H. E. (1998). *Nature (London)*, **396**, 329–335.
Moss, G. W., Lieb, W. R. & Franks, N. P. (1991). *Biophys. J.* **60**, 1309–1314.
Murshudov, G. N., Vagin, A. A. & Dodson, E. J. (1997). *Acta Cryst.* D**53**, 240–255.
Refaee, M., Tezuka, T., Akasaka, K. & Williamson, M. P. (2003). *J. Mol. Biol.* **327**, 857–865.
Rodgers, D. W. (1994). *Structure*, **2**, 1135–1140.
Röttger, K., Endriss, A., Ihringer, J., Doyle, S. & Kuhs, W. F. (1994). *Acta Cryst.* B**50**, 644–648.
Steller, I., Bolotovsky, R. & Rossman, M. G. (1997). *J. Appl. Cryst.* **30**, 1036–1040.
Thomanek, U. F., Parak, F., Mössbauer, R. L., Formanek, H., Schwager, P. & Hoppe, W. (1973). *Acta Cryst.* A**29**, 263–265.
Unno, M., Ishimori, K. & Morishima, I. (1990). *Biochemistry*, **29**, 10199–10205.
Urayama, P., George, N. P. & Gruner, S. M. (2002). *Structure*, **10**, 51–60.
Vagin, A. & Teplyakov, A. (1997). *J. Appl. Cryst.* **30**, 1022–1025.
Verkhusha, V. V., Pozhitkov, A. E., Smirnov, S. A., Borst, J. W., Hoek, A., Klyachko, N. L., Levashov, A. V. & Visser, A. J. W. G. (2003). *Biochim. Biophys. Acta*, **1622**, 192–195.
Watowich, S. J., Skehel, J. J. & Wiley, D. C. (1995). *Acta Cryst.* D**51**, 7–12.
Weber, G. & Drickamer, H. G. (1983). *Q. Rev. Biophys.* **16**, 89–112.
Young, A. C. M., Dewan, J. C., Nave, C. & Tilton, R. F. (1993). *J. Appl. Cryst.* **26**, 309–319.
Zhang, H., Teng, M., Niu, L., Wang, Y., Wang, Y., Liu, Q., Huang, Q., Hao, Q., Dong, Y. & Liu, P. (2004). *Acta Cryst.* D**60**, 974–977.